

# ROTATING STRATIFIED TURBULENCE WITH VERTICAL AND NON-VERTICAL SHEAR

Frank G. Jacobitz  
Mechanical Engineering Program  
University of San Diego  
5998 Alcalá Park, San Diego, CA 92110, USA  
jacobitz@sandiego.edu

## ABSTRACT

Direct numerical simulations are performed to investigate the effect of stratification, shear, and rotation, on the evolution of homogeneous turbulence. This study considers uniform vertical stable stratification as well as vertical and non-vertical shear and system rotation. The rotation axis is always normal to the plane of shear and it is therefore parallel or anti-parallel to the mean flow vorticity. Three parameters are used to characterize the flow: the Richardson number  $Ri = N^2/S^2$ , which is the square of the ratio of Brunt-Väisälä frequency  $N$  to shear rate  $S$ , the rotation ratio  $f/S$ , which is the ratio of Coriolis parameter  $f$  to shear rate  $S$ , and the shear angle  $\theta$  between the plane of shear and the vertical. An increase of the Richardson number  $Ri$  leads to weakened growth of the turbulent kinetic energy  $K$ . In the anti-parallel flow configuration, turbulence growth is amplified for rotation ratios between  $0 < f/S < 1$  and weakened otherwise. For  $f/S = 0.5$  the value of the critical Richardson number  $Ri_{cr}$ , which distinguishes turbulence growth from decay, exceeds the classical value of a quarter obtained from linear inviscid stability theory. In the parallel flow configuration, the turbulence is weakened by rotation for all values of the rotation ratio  $f/S$ . Non-vertical shear generally leads to stronger turbulence growth. This effect is strongest in the anti-parallel flow configuration and weakest in the parallel flow configuration.

## INTRODUCTION

Stable density stratification, shear, and system rotation are ubiquitous features of flows with many applications (for example Miesch, 2005). The flow considered here has uniform vertical stable stratification with constant stratification rate  $S_\rho = \partial \varrho / \partial z$ , uniform shear with constant shear rate  $S$  inclined at an angle  $\theta$  to the vertical direction, and system rotation about an axis normal to the plane of shear with constant Coriolis parameter  $f = 2\Omega$ :

$$\begin{aligned}\varrho &= \rho_0 + S_\rho z \\ U &= S \sin \theta y + S \cos \theta z \\ V &= W = 0\end{aligned}$$

The Cartesian coordinates  $x$ ,  $y$ , and  $z$  refer to the downstream, spanwise, and vertical directions, respectively.

Turbulence in a stably stratified fluid has been studied extensively in the past, both experimentally (Itsweire, Helland and Van Atta, 1986; Yoon and Warhaft, 1990) and numerically (Riley, Metcalfe and Weissman, 1981; Métais and Herring, 1989). Similarly, extensive work has been performed to understand turbulent stratified shear flows (Komori, Ueda, Ogino and Mizushima, 1983; Rohr, Itsweire, Helland and Van Atta, 1988; Piccirillo and Van Atta, 1997;

Gerz, Schumann and Elghobashi, 1989; Holt, Koseff and Ferziger, 1992; Jacobitz, Sarkar and Van Atta, 1997). Non-vertical shear in vertically stably stratified flows has been considered by Jacobitz and Sarkar (1998) and Jacobitz (2002).

Studies of rotating shear flows have focused on the case with the rotation axis normal to the plane of shear and therefore parallel or anti-parallel to the mean flow vorticity. In the anti-parallel case the effect of rotation was found to be destabilizing for  $0 < f/S < 1$  and stabilizing otherwise (Bradshaw, 1969; Tritton, 1992). Linear theory has been used by Salhi (2002) to investigate the similarities of rotation and stratification in such flows. A comprehensive investigation of this flow was performed recently by Brethouwer (2005).

The purpose of this study is to study the effects of stratification, shear, and rotation on the evolution of turbulence and to extend existing results to non-vertical shear and rotation. In the next section, the numerical approach is summarized. Then simulation results are presented in which the Richardson number  $Ri$ , the rotation ratio  $f/S$ , and the shear angle  $\theta$  are varied. Finally, the main results of this study are summarized.

## NUMERICAL APPROACH

The direct numerical simulations performed here are based on the continuity equation for an incompressible fluid, the unsteady three-dimensional Navier-Stokes equation in the Boussinesq approximation, and an advection-diffusion equation for the density. In the direct numerical approach, all dynamically important scales of the velocity and density fields are resolved. The equations are solved in a frame of reference moving with the mean flow (Rogallo, 1981). This approach allows the use of periodic boundary conditions for the fluctuating components of the velocity and density fields. A spectral collocation method is used for the spatial discretization and the solution is advanced in time with a fourth-order Runge-Kutta scheme. The simulations are performed on a parallel computer using a grid with  $256 \times 256 \times 256$  points.

## RESULTS

In this section, the results from direct numerical simulations of stably stratified, rotating shear flows are presented. First, stratified shear flow is considered and the Richardson number is varied from  $Ri = 0$  to  $Ri = 1$ . Second, rotating shear flow is considered and the rotation ratio is varied from  $f/S = 0$  to  $f/S = 10$ . Third, results from simulations of rotating stratified shear flow are presented. Finally, results from simulations with non-vertical shear and rotation

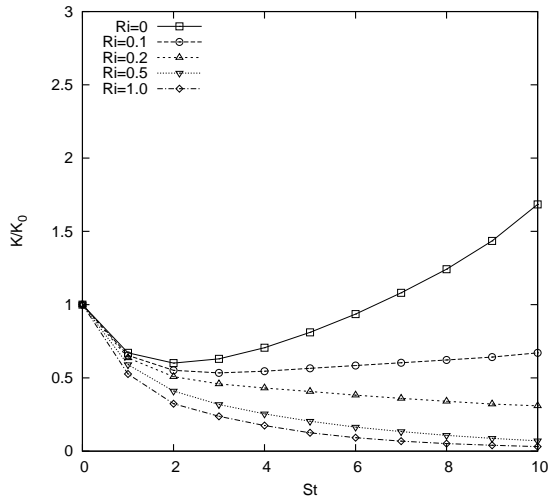


Figure 1: Evolution of the normalized turbulent kinetic energy  $K/K_0$  with non-dimensional time  $St$ . The Richardson number is varied from  $Ri = 0$  (unstratified) to  $Ri = 1$  (strongly stratified). The rotation ratio is  $f/S = 0$  and the stratification angle is  $\theta = 0$ .

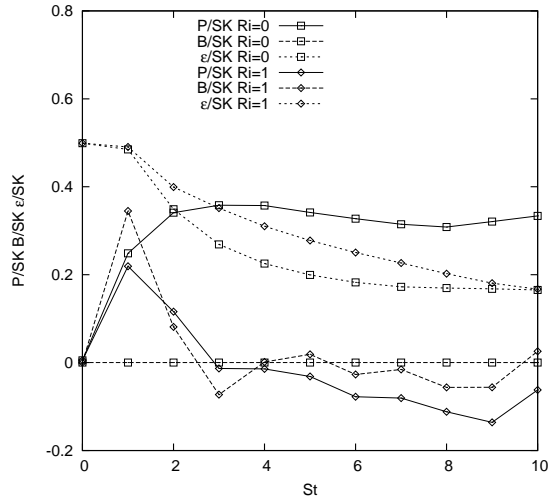


Figure 2: Evolution of the normalized production rate  $P/SK$ , buoyancy flux  $B/SK$  and dissipation rate  $\epsilon/SK$  with non-dimensional time  $St$ . Two cases with  $Ri = 0$  and  $Ri = 1$  are shown. The rotation ratio is  $f/S = 0$  and the stratification angle is  $\theta = 0$ .

are discussed and the shear angle is varied from  $\theta = 0^\circ$  to  $\theta = 90^\circ$ .

All simulations are initialized with isotropic turbulence fields without density fluctuations. The initial Taylor microscale Reynolds number  $Re_\lambda = 45$  and the initial shear number  $SK/\epsilon = 2$  are matched in all cases. The molecular Prandtl number of the density field is  $Pr = 0.7$ .

### Stratified Shear Flow

In this section, results from a series of simulations of stably stratified shear flow are presented. The Richardson number  $Ri$  is varied from  $Ri = 0$ , corresponding to unstratified shear flow, to  $Ri = 1$ , corresponding to strongly stratified shear flow. There is no rotation ( $f/S = 0$ ) and the shear is vertical ( $\theta = 0$ ).

Figure 1 shows the evolution of the turbulent kinetic en-

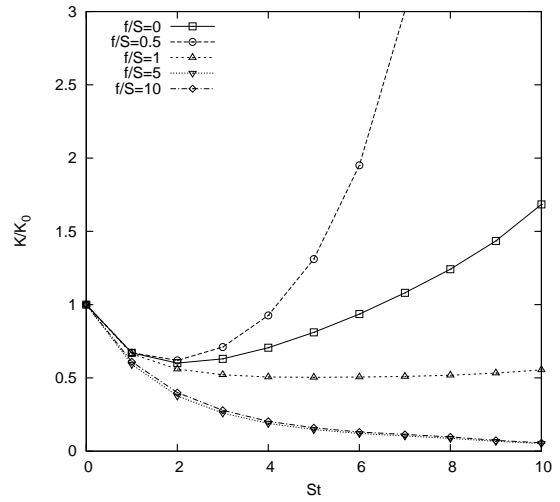


Figure 3: Evolution of the normalized turbulent kinetic energy  $K/K_0$  with non-dimensional time  $St$ . The rotation ratio is varied from  $f/S = 0$  to  $f/S = 10$ . The configuration is anti-parallel. The Richardson number is  $Ri = 0$  and the stratification angle is  $\theta = 0$ .

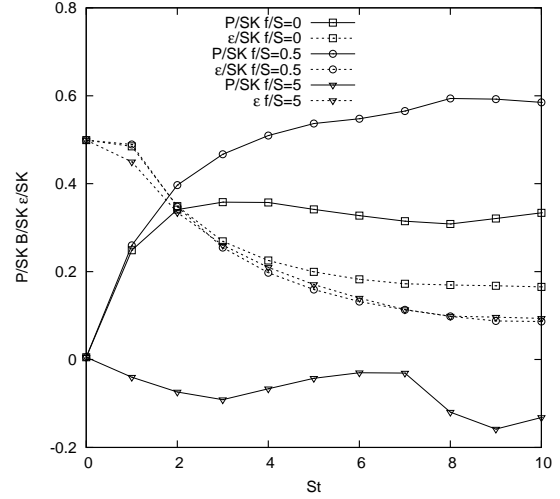


Figure 4: Evolution of the normalized production rate  $P/SK$  and dissipation rate  $\epsilon/SK$  with non-dimensional time  $St$ . The rotation ratio is varied from  $f/S = 0$  to  $f/S = 10$ . The configuration is anti-parallel. The Richardson number is  $Ri = 0$  and the stratification angle is  $\theta = 0$ .

ergy  $K = \overline{u_i u_i} / 2$  with non-dimensional time  $St$ . Initially, the turbulent kinetic energy decays due to the isotropic initial conditions until the shear production of turbulence develops at about  $St = 2$ . For strongly stratified cases with Richardson numbers  $Ri \geq 0.2$ , the turbulent kinetic energy continues to decay. For weakly stratified cases with  $Ri \leq 0.1$ , the turbulent kinetic energy eventually grows as the simulations advance. Note that the value of the critical Richardson number  $Ri_{cr} \approx 0.15$  observed here is somewhat smaller than the value of one quarter determined from linear inviscid stability theory by Miles (1961) and Howard (1961).

The transport equation for the turbulent kinetic energy equation can be written in the following non-dimensional form:

$$\gamma = \frac{1}{SK} \frac{dK}{dt} = \frac{P}{SK} - \frac{B}{SK} - \frac{\epsilon}{SK} \quad (1)$$

Here  $P = -S\overline{uw}$  is the production rate,  $B = g\overline{w\rho} / \rho_0$  is the

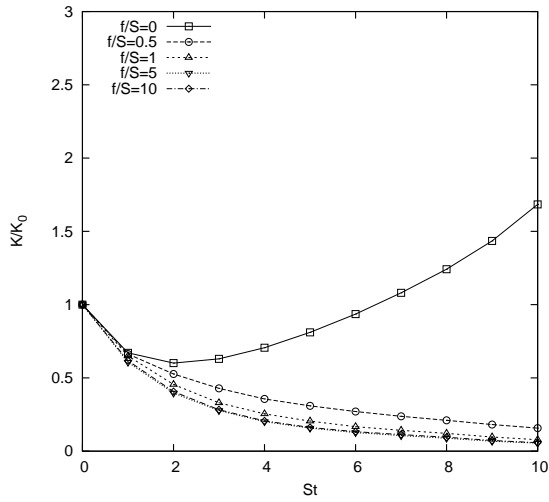


Figure 5: Evolution of the normalized turbulent kinetic energy  $K/K_0$  with non-dimensional time  $St$ . The rotation ratio is varied from  $f/S = 0$  to  $f/S = 10$ . The configuration is parallel. The Richardson number is  $Ri = 0$  and the stratification angle is  $\theta = 0$ .

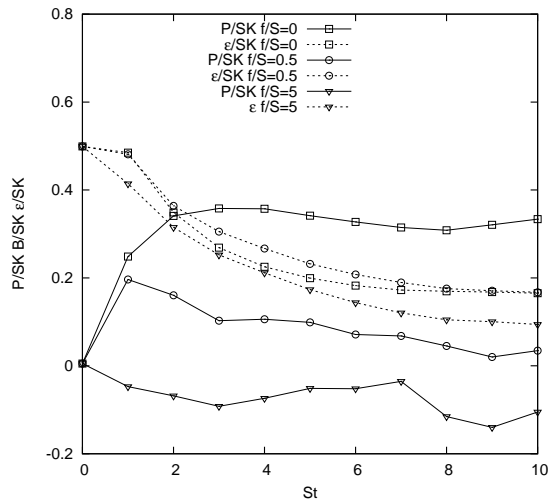


Figure 6: Evolution of the normalized production rate  $P/SK$  and dissipation rate  $\epsilon/SK$  with non-dimensional time  $St$ . The rotation ratio is varied from  $f/S = 0$  to  $f/S = 10$ . The configuration is parallel. The Richardson number is  $Ri = 0$  and the stratification angle is  $\theta = 0$ .

buoyancy flux, and  $\epsilon$  is the viscous dissipation rate. This equation defines the growth rate  $\gamma$  of the turbulent kinetic energy.

Figure 2 shows the evolution of the normalized production rate  $P/SK$ , buoyancy flux  $B/SK$ , and dissipation rate  $\epsilon/SK$  for two simulations with  $Ri = 0$  and  $Ri = 1$ . As the Richardson number is increased, the normalized production rate  $P/SK$  decreases strongly, resulting in decay of the turbulent kinetic energy. In the unstratified case with  $Ri = 0$ , the normalized production rate  $P/SK$  is positive. Similarly, in weakly stratified cases, both  $P/SK$  and  $B/SK$  are positive, indicating down-gradient fluxes (not shown here). Both  $P/SK$  and  $B/SK$  are negative in the strongly stratified case with  $Ri = 1$  and the fluxes are counter-gradient. A more extensive discussion of the energetics of stably stratified shear flow can be found in Jacobitz *et al.* (1997).

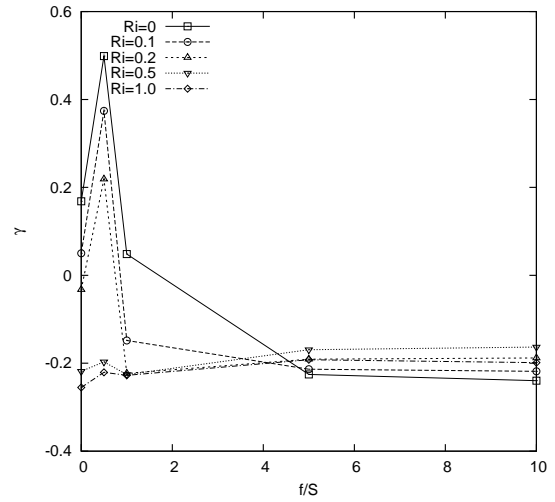


Figure 7: Dependence of the growth rate  $\gamma$  of the turbulent kinetic energy  $K$  on the rotation ratio  $f/S$  and the Richardson number  $Ri$  at non-dimensional time  $St = 10$ . The configuration is anti-parallel and the stratification angle is  $\theta = 0$ .

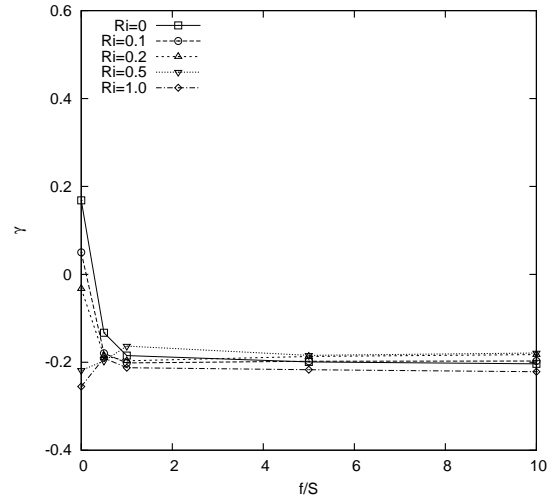


Figure 8: Dependence of the growth rate  $\gamma$  of the turbulent kinetic energy  $K$  on the rotation ratio  $f/S$  and the Richardson number  $Ri$  at non-dimensional time  $St = 10$ . The configuration is parallel and the stratification angle is  $\theta = 0$ .

### Rotating Shear Flow

This section discusses the effect of rotation on the evolution of turbulence in shear flow. The rotation ratio is varied from  $f/S = 0$ , corresponding to non-rotating shear flow, to  $f/S = 10$ , corresponding to strongly rotating shear flow. Both parallel and anti-parallel cases are considered, in which the vorticity of the system rotation and mean flows are directed in the same or opposite direction, respectively. There is no stratification ( $Ri = 0$ ) and the shear is vertical ( $\theta = 0$ ).

Figure 3 shows the evolution of the turbulent kinetic energy  $K$  with non-dimensional time  $St$  for the anti-parallel configuration. The case without rotation ( $f/S = 0$ ) was already included in the discussion of the Richardson number variation. The moderately rotating case with  $f/S = 0.5$  shows strongly increased growth of the turbulent kinetic energy  $K$ . A further increase of the rotation ratio beyond  $f/S > 1$  leads to decay of the turbulent kinetic energy.

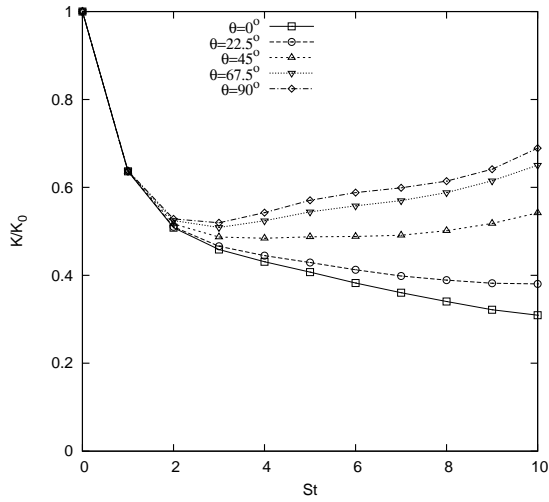


Figure 9: Evolution of the normalized turbulent kinetic energy  $K/K_0$  with non-dimensional time  $St$ . The shear angle is varied from  $\theta = 0$  (vertical shear) to  $\theta = 90^\circ$  (horizontal shear). The Richardson number is  $Ri = 0.2$  and the rotation ratio is  $f/S = 0$ .

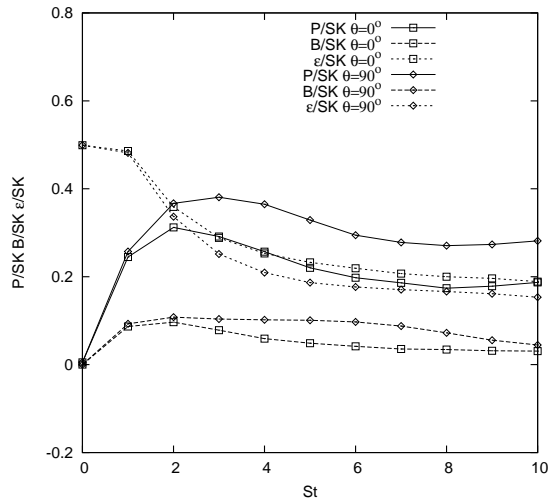


Figure 10: Evolution of the normalized production rate  $P/SK$ , buoyancy flux  $B/SK$ , and dissipation rate  $\epsilon/SK$  with non-dimensional time  $St$ . The shear angle is varied from  $\theta = 0$  to  $\theta = 90^\circ$ . The Richardson number is  $Ri = 0.2$  and the rotation ratio is  $f/S = 0$ .

Figure 4 shows the evolution of the normalized production rate  $P/SK$  and dissipation rate  $\epsilon/SK$  for three simulations with  $f/S = 0$  (squares),  $f/S = 0.5$  (circles), and  $f/S = 5$  (triangles). Note that there is no buoyancy flux  $B/SK$  in the unstratified cases. Rotation only slightly affects the normalized dissipation rate  $\epsilon/SK$ , but strongly increases the normalized production rate  $P/SK$  as the rotation rate is increased from  $f/S = 0$  to  $f/S = 0.5$  and finally decreases  $P/SK$  with a further increase to  $f/S = 5$ . The primary mechanism to affect the energetics of the flow is the impact of rotation on the turbulence production rate.

Figure 5 shows the evolution of the turbulent kinetic energy  $K$  with non-dimensional time  $St$  for the parallel configuration. An increase of the rotation ratio  $f/S$  leads to an increased decay of the turbulent kinetic energy  $K$ .

Figure 6 shows the evolution of the normalized produc-

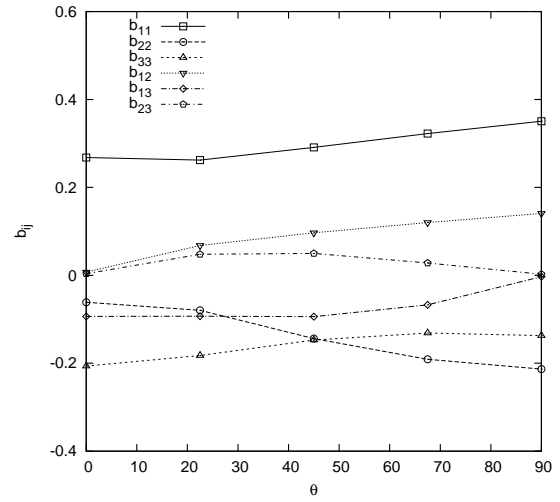


Figure 11: Dependence of the components of the anisotropy tensor  $b_{ij}$  on the shear angle  $\theta$  at non-dimensional time  $St = 10$ . The shear angle is varied from  $\theta = 0$  to  $\theta = 90^\circ$ . The Richardson number is  $Ri = 0.2$  and the rotation ratio is  $f/S = 0$ .

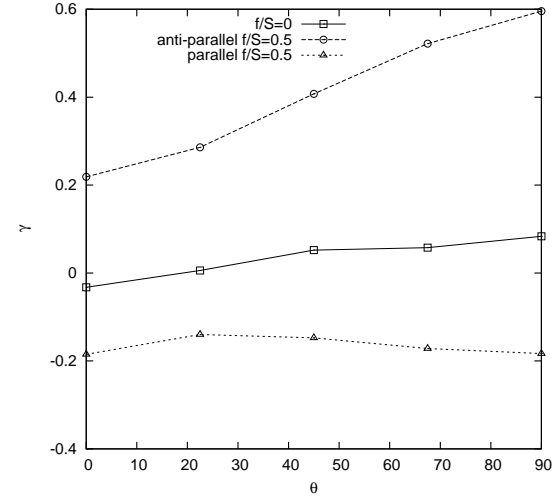


Figure 12: Dependence of the growth rate  $\gamma$  on the shear angle  $\theta$  and the rotation ratio  $f/S$  at non-dimensional time  $St = 10$ . Both parallel and anti-parallel configurations are shown. The rotation ratio is  $f/S = 0.5$  and the Richardson number is  $Ri = 0.2$ .

tion rate  $P/SK$  and dissipation rate  $\epsilon/SK$  for three simulations with  $f/S = 0$  (squares),  $f/S = 0.5$  (circles), and  $f/S = 5$  (triangles). Again, rotation only slightly affects the normalized dissipation rate  $\epsilon/SK$ , but strongly decreases the normalized production rate  $P/SK$  as the rotation rate  $f/S$  is increased.

### Rotating Stratified Shear Flow

This section discusses the effects of both stratification and rotation on turbulent shear flow. The Richardson number is varied from  $Ri = 0$  to  $Ri = 1$  and the rotation number is varied from  $f/S = 0$  to  $f/S = 10$ . Both parallel and anti-parallel flow configurations are considered. The shear remains in the vertical direction ( $\theta = 0$ ).

Figure 7 shows the values of the growth rate  $\gamma = P/SK - B/SK - \epsilon/SK$  at the end of the simulations at

non-dimensional time  $St = 10$  for the anti-parallel flow configuration. A positive value of the growth rate  $\gamma$  corresponds to eventual growth of the turbulent kinetic energy  $K$  and a negative value corresponds to decay of the turbulent kinetic energy. For  $f/S = 0$  the growth rates of non-rotating stratified shear flow are obtained. With increasing Richardson number  $Ri$ , the growth rates  $\gamma$  decrease and switch sign as the turbulent kinetic energy evolution changes from growth to decay. For  $f/S = 0.5$  the growth rates are strongly increased compared to the non-rotating case. A further increase of the rotation ratio  $f/S$  leads to smaller values of the growth rate  $\gamma$ . The two strongly rotating cases with  $f/S = 5$  and  $f/S = 10$  show almost no change in the respective values of  $\gamma$ . For these two cases decay of the turbulent kinetic energy is always observed, irrespective of the value of the Richardson number  $Ri$ .

Figure 8 shows the values of the growth rate  $\gamma$  at non-dimensional time  $St = 10$  for the parallel flow configuration. As the rotation ratio is increased from  $f/S = 0$  to  $f/S = 0.5$ , the growth rate of the weakly stratified cases with  $Ri = 0$ ,  $Ri = 0.1$ , and  $Ri = 0.2$  decrease substantially. Only the growth rates of the strongly stratified cases with  $Ri = 0.5$  and  $Ri = 1$  increase slightly, but remain negative. For larger rotation ratios  $f/S \geq 1$  the growth rates of all cases remain negative and almost constant.

The dependence of the growth rate  $\gamma$  on the rotation ratio has an important impact on the value of the critical Richardson number  $Ri_{cr}$ . The critical Richardson number  $Ri_{cr}$  distinguishes regimes of turbulence growth with positive  $\gamma$  from those of decay with negative  $\gamma$ . The critical value of the Richardson number is obtained for cases with constant turbulent kinetic energy and  $\gamma = 0$ . For the anti-parallel flow configuration the  $f/S = 0.5$  case results in a critical Richardson number of about  $Ri_{cr} = 0.32$ . Note that this value is clearly above the classical value of  $Ri_{cr} = 0.25$  obtained by Miles (1961) and Howard (1961) using linear inviscid stability theory.

### Non-vertical shear and rotation

This section discusses the effect of an angle  $\theta$  between the vertical direction of stratification and the plane of shear. Note that in all cases the axis of rotation remains normal to the plane of shear and therefore parallel or anti-parallel to the mean flow vorticity.

Figure 9 shows the evolution of the turbulent kinetic energy  $K$  in non-dimensional time  $St$ . The shear angle is varied from  $\theta = 0$ , corresponding to vertical shear, to  $\theta = 90^\circ$ , corresponding to horizontal shear. The flow is stratified with  $Ri = 0.2$  and there is no rotation with  $f/S = 0$ . As the shear angle is increased, the evolution of the turbulent kinetic energy changes from decay for  $\theta = 0$  and  $\theta = 22.5^\circ$  to growth for  $\theta = 45^\circ$ ,  $\theta = 67.5^\circ$ , and  $\theta = 90^\circ$ .

Figure 10 shows the evolution of the normalized production rate  $P/SK$ , buoyancy flux  $B/SK$ , and dissipation rate  $\epsilon/SK$  in non-dimensional time  $St$  for vertical shear with  $\theta = 0$  (squares) and for horizontal shear with  $\theta = 90^\circ$  (diamonds). The strongest impact of the shear angle variation is an increase of the turbulence production rate  $P/SK$ . This increase is due to a decreased influence of buoyancy on the horizontal shear production component (Jacobitz, 2002). The impact of a shear angle variation on the normalized buoyancy flux  $B/SK$  and dissipation rate  $\epsilon/SK$  is smaller.

Figure 11 shows the components of the shear stress anisotropy tensor  $b_{ij} = \overline{u_i u_j} / \overline{u_k u_k} - \delta_{ij}/3$  at non-dimensional time  $St = 10$ . The diagonal components de-

scribe the distribution of the turbulent kinetic energy. In the vertical shear case ( $\theta = 0$ ) the components are ordered  $b_{11} > b_{22} > b_{33}$  or downstream  $>$  spanwise  $>$  vertical. As the shear angle is increased, the downstream component  $b_{11}$  remains relatively unaffected. The spanwise component  $b_{22}$  and vertical component  $b_{33}$  follow different trends:  $b_{22}$  decreases and  $b_{33}$  increases. In the horizontal shear case ( $\theta = 90^\circ$ ), the components are ordered  $b_{11} > b_{33} > b_{22}$  or downstream  $>$  vertical  $>$  spanwise.

The off-diagonal component  $b_{13}$  is a direct measure for the production of turbulent kinetic energy due to vertical shear. It reduces to zero for  $\theta = 90^\circ$ . The component  $b_{12}$  is a direct measure for the production of turbulence due to horizontal shear. It assumes a zero value only for  $\theta = 0$ . The final component  $b_{23}$  is zero for  $\theta = 0$  and  $\theta = 90^\circ$  due to symmetry of the flow. For other angles it assumes a small non-zero value.

Figure 12 shows the dependence of the growth rate  $\gamma$  on the shear angle  $\theta$  at non-dimensional time  $St = 10$ . In the non-rotating case with  $f/S = 0$  the growth rate is negative for vertical shear ( $\theta = 0$ ), increases with  $\theta$ , and eventually reaches a positive value for  $\theta = 90^\circ$ . In the anti-parallel case with  $f/S = 0.5$  a similar result is found. The growth rate  $\gamma$  increases with the shear angle  $\theta$ . All growth rates are positive and the effect is stronger compared to the non-rotating case. In the parallel case with  $f/S = 0.5$ , all growth rates are negative and the growth rate remains almost constant over the full range of shear angle variation.

### SUMMARY

Direct numerical simulations of the evolution of stably stratified, sheared, and rotating turbulence have been performed. The simulations consider vertical stable density stratification as well as vertical and non-vertical shear and rotation. In all cases the rotation axis is parallel or anti-parallel to the mean flow vorticity. The Richardson number was varied from  $Ri = 0$  to  $Ri = 1$  and the growth of the turbulent kinetic energy  $K$  weakens as an increase of the Richardson number leads to a decrease of the normalized turbulence production rate. The rotation ratio was varied from  $f/S = 0$  to  $f/S = 10$  for both the parallel and anti-parallel flow configuration. For the anti-parallel flow configuration, the turbulence growth is strengthened for rotation ratios  $0 < f/S < 1$  and weakened for larger values. For  $f/S = 0.5$  the critical Richardson number  $Ri_{cr}$ , which distinguishes regimes of turbulence growth and decay, was observed to exceed the classical value of one quarter obtained from linear inviscid stability theory. In the parallel flow configuration, weaker turbulence growth is found for all values of the rotation ratio  $f/S$ . Non-vertical shear generally results in stronger turbulence growth due to an increased turbulence production from the horizontal shear component that is not directly affected by buoyancy. This effect is strongest for the anti-parallel flow configuration.

### ACKNOWLEDGMENTS

This project is supported with computer time by the National Partnership for Advanced Computational Infrastructure and direct numerical simulations were performed at the facilities of the San Diego Supercomputer Center. I would like to express many thanks for ongoing discussions of turbulence to Marie Farge, Lukas Liechtenstein, and Kai Schneider.

## REFERENCES

- Bradshaw, P., 1969, "The analogy between streamline curvature and buoyancy in turbulent shear flow", *J. Fluid Mech.*, Vol. 36, pp. 177–191.
- Brethouwer, G., 2005, "The effect of rotation on rapidly sheared homogeneous turbulence and passive scalar transport. Linear theory and direct numerical simulations", *J. Fluid Mech.*, Vol. 542, pp. 305–342.
- Gerz, T., Schumann, U., and Elghobashi, S.E., 1989, "Direct numerical simulation of stratified homogeneous turbulent shear flows", *J. Fluid Mech.*, Vol. 200, pp. 563–594.
- Holt, S.E., Koseff, J.R., and Ferziger, J.H., 1992, "A numerical study of the evolution and structure of homogeneous stably stratified sheared turbulence", *J. Fluid Mech.*, Vol. 237, pp. 499–539.
- Howard, L.N., 1961, "Note on a paper of John W. Miles", *J. Fluid Mech.*, Vol. 10, pp. 509–512.
- Itsweire, E.C., Helland, K.N., and Van Atta, C.W., 1986, "The evolution of grid-generated turbulence in a stably stratified fluid", *J. Fluid Mech.*, Vol. 162, pp. 299–338.
- Jacobitz, F.G., Sarkar, S., and Van Atta, C.W., 1997, "Direct numerical simulations of the turbulence evolution in a uniformly sheared and stably stratified flow", *J. Fluid Mech.*, Vol. 342, pp. 231–261.
- Jacobitz, F.G., and Sarkar, S., 1998, "The effect of non-vertical shear on turbulence in a stably stratified medium", *Phys. Fluids*, Vol. 10, pp. 1158–1168.
- Jacobitz, F.G., 2002, "A comparison of the turbulence evolution in a stratified fluid with vertical or horizontal shear", *J. Turbulence*, Vol. 3, pp. 55, 1–16.
- Komori, S., Ueda, H., Ogino, F., and Mizushima, T., 1983, "Turbulence structure in stably stratified open-channel flow", *J. Fluid Mech.*, Vol. 130, pp. 13–26.
- Métais, O., and Herring, J., 1989, "Numerical simulations of freely evolving turbulence in stably stratified fluids", *J. Fluid Mech.*, Vol. 202, pp. 117–148.
- Miesch, M.S., 2005, "Large-scale dynamics of the convection zone and tachocline", *Living Rev. Solar Phys.*, Vol. 2, pp. 1.
- Miles, J.W., 1961, "On the stability of heterogeneous shear flows", *J. Fluid Mech.*, Vol. 10, pp. 496–508.
- Piccirillo, P.S., and Van Atta, C.W., 1997, "The evolution of a uniformly sheared thermally stratified turbulent flow", *J. Fluid Mech.*, Vol. 334, pp. 61–86.
- Riley, J.J., Metcalfe, R.W., and Weissman, M.A., 1981, "Direct numerical simulations of homogeneous turbulence in density stratified fluids", *Nonlinear Properties of Internal Waves*, AIP Conference Proceedings, Vol. 76, pp. 79–112.
- Rogallo, R.S., 1981, "Numerical experiments in homogeneous turbulence", Technical Memorandum 81315, NASA Ames Research Center, Moffett Field, CA.
- Rohr, J.J., Itsweire, E.C., Helland, K.N., and Van Atta, C.W., 1988, "Growth and decay of turbulence in a stably stratified shear flow", *J. Fluid Mech.*, Vol. 195, pp. 77–111.
- Salhi, A., 2002, "Similarities between rotation and stratification effects on homogeneous shear flow", *Theoret. Comp. Fluid Dyn.*, Vol. 15, pp. 339–358.
- Tritton, D.J., 1992, "Stabilization and destabilization of turbulent shear flow in a rotating fluid", *J. Fluid Mech.*, Vol. 241, pp. 503–523.
- Yoon, K., and Warhaft, Z., 1990, "The evolution of grid-generated turbulence under conditions of stable thermal stratification", *J. Fluid Mech.*, Vol. 215, pp. 601–638.